Large-angle correlations between ^{4}He and ^{1,2,3}H or ^{4}He in the reactions 247 and 337 MeV ^{40}Ar+^{nat}Ag: Unexpected properties of the nuclear stratosphere

Roy Lacey, N. N. Ajitanand,* John M. Alexander, D. M. de Castro Rizzo, G. F. Peaslee, and L. C. Vaz
Department of Chemistry, State University of New York at Stony Brook, Stony Brook, New York 11794

Morton Kaplan, M. Kildir,† G. La Rana,‡ D. J. Moses, and W. E. Parker
Department of Chemistry, Carnegie-Mellon University, Pittsburgh, Pennsylvania 15213

D. Logan§ and M. S. Zisman
Lawrence Berkeley Laboratory, Berkeley, California 94720

P. DeYoung**
Department of Physics, State University of New York at Stony Brook, Stony Brook, New York 11794

L. Kowalski
Department of Physics and Geoscience, Montclair State College, Upper Montclair, New Jersey 07043
(Received 11 February 1988)

We have measured coincidences between ^{4}He and ^{1,2,3}H or a second ^{4}He (large-angle correlations) in the reactions 247 and 337 MeV ^{40}Ar+^{nat}Ag. These coincidences are dominated by reactions leading to evaporation residues with spins of about 0–70$\hbar$. Large values of the angle-integrated double and triple coincidence cross sections indicate that many particle evaporation chains involve 2 or 3 protons and/or 2 or 3 alphas. The angular and energy distributions are well described by an evaporation model with Hauser-Feshbach coupling. However, one must employ effective evaporation barriers for ^{1}H and ^{4}He that are strongly reduced compared to empirical fusion barriers. The barrier reduction required for ^{2}H is rather small, and for ^{3}H no barrier reduction is needed. Evaporation calculations that include emitter deformation do not give a satisfactory explanation for these results. We suggest a new aspect of composite nucleus excitation and evaporation-like decay. A hot, very diffuse nuclear surface may be formed that promotes evaporative decay prior to its relaxation. The low barriers for ^{1}H and ^{4}He reflect the radial extent of this transitory, diffuse surface.

I. INTRODUCTION

Reactions between heavy nuclei of energy $\lesssim 20$ MeV per nucleon are particularly effective for producing hot, thermally equilibrated composite nuclei. Decay of these composite systems gives a profusion of evaporated light particles and (for heavier systems) nuclear fission. The reactions 247 and 337 MeV ^{40}Ar+^{107,9}Ag have been shown to give evaporation residues (ER), fusion fission (FF), and quasifission (QF) products in comparable abundance.[1] Measured cross sections indicate that the ER's are populated by entrance channel spins of about $\approx 0-l_{ER}$ [$l_{ER}=68(70)\hbar$ for 247 (337) MeV ^{40}Ar]. Thus, the particle spectra associated with these residues contain information about the hot composite nuclei formed in this group of rather central collisions. Such particle spectra have been often measured in singles, and more recently in coincidence with ER's,[2] γ rays[3] or a second particle.[4–6]

In a companion study[7] we have presented measurements (for 247 and 337 MeV ^{40}Ar+^{nat}Ag) in singles and in coincidence with fusion-fission and quasifission. These data indicate that most evaporative ^{1}H and ^{4}He particles are produced by chains leading to the ER's. Indeed the average chain lengths for these particles are significantly less than unity when observed in association with FF or QF but substantially greater than unity for the ER's. This result suggests that the detection of particle-particle coincidences can select out the ER chains. In addition, reaction simulation calculations[8,9] indicate that such coincidence data are essentially insensitive to recoil effects (purely kinematic) while they put quite interesting constraints on the emitter spin, moment of inertia, temperature, shape, and size.

In this paper we present results obtained from particle-particle coincidences involving ^{1,2,3}H and ^{4}He. We give evidence that these particles are emitted from completely fused and thermalized composite nuclei. We also determine angle-integrated cross sections for double coincidences ($\alpha\alpha$, pp, and pα) as well as triple coincidences between three particles ($\alpha\alpha\alpha$, ppp, p$\alpha\alpha$, and αpp) and between one fragment (f) and two particles ($f\alpha\alpha$, $f$pp, and $f\alpha$p). From these results we get information on the particular emission chains that lead to ER's. The observed energy and angular distributions are compared to reaction simulation calculations based on statistical theory. The "standard model"[10–14] accounts for these angular distributions very well. By contrast the en-

ergy distributions reveal deviations from the statistical model that have very interesting and puzzling trends. Our interpretation of these trends is that particle evaporation occurs from the fringes of a transitory nuclear stratosphere prior to its relaxation. A brief report of some of these results has already been published.[5,6]

II. EXPERIMENTAL SETUP AND OBJECTIVES

In a preceding paper[7] we have described a number of the experimental details for this study. In short, we bombarded natural Ag targets with ^{40}Ar beams of 247 and 337 MeV, provided by the Berkeley superHILAC. The detection geometry for one of three experiments is shown in Fig. 1(a). Alpha particles were measured from 65° to 155° in two wedge detectors,[15] each with an ionization chamber for ΔE signals and five Si stopping detectors. Coincidence triggers [S-1, 2, and 3 in Fig. 1(a)] were provided by three solid state telescopes (SST) (50 μm, 500 μm, 5 mm) for ^{1,2,3}H and ^{4}He. Three additional coincidence triggers for fissionlike fragments were provided by gas ionization telescopes (GT).[16] Results for the fragment-particle coincidences and the singles are given in Ref. 7. In this paper we focus on the particle-particle coincidences.

A schematic idealization of the geometry is shown in Fig. 1(b). After transformation into the c.m. system, the SST triggers are very close to 90 deg from the beam.

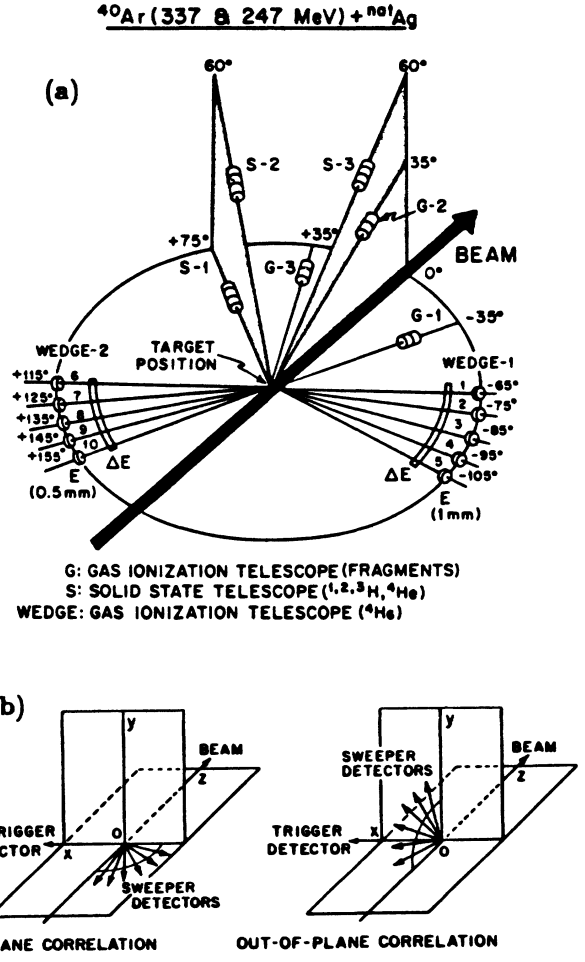

FIG. 1. (a) Schematic diagram of the experimental setup in the laboratory. (b) Schematic diagram for idealized in-plane and out-of-plane correlations in the c.m. For particle-particle correlations the former employs S-1 as trigger, while the latter employs S-3 as trigger.

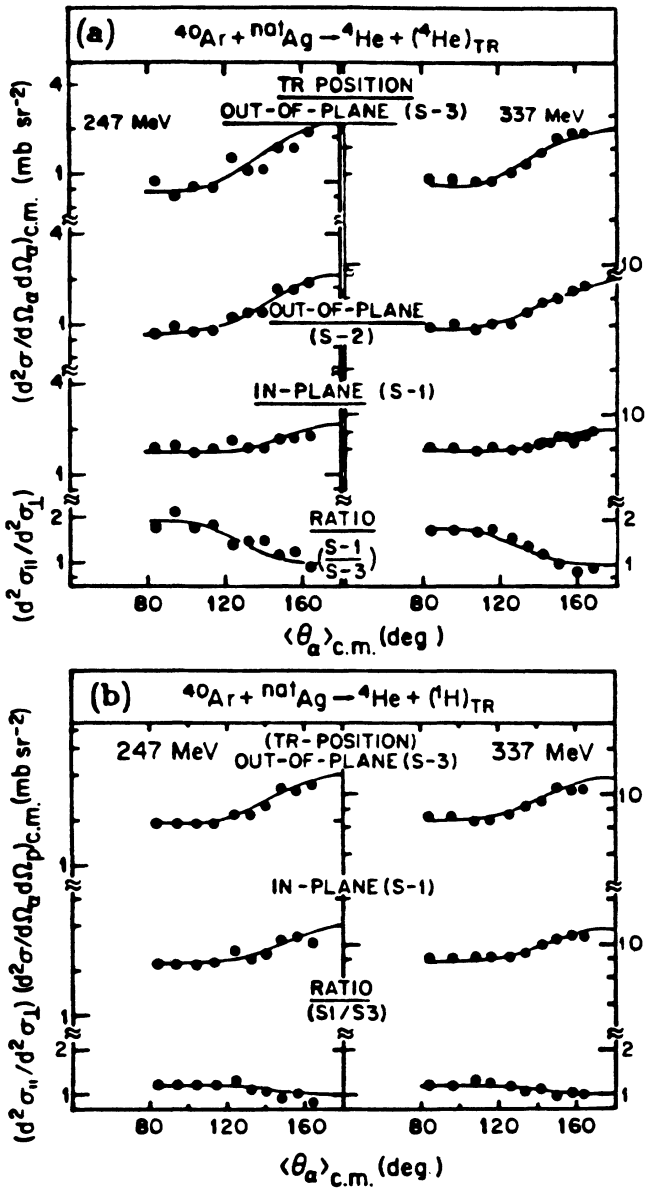

FIG. 2. (a) Measured angular correlations for ^{4}He in coincidence with the ^{4}He trigger. Solid curves were calculated for spherical emitters with initial spin zone $35 < J < l_{ER}$ and mean excitation energy $\frac{2}{3}$ of that calculated for the compound nucleus (E_{CN}). (b) Measured angular correlations for ^{4}He in coincidence with the ^{1}H trigger. Solid curves were calculated with initial spin zone of $0 < J < 70\hbar$ (or $J_{rms} = 50\hbar$) and mean excitation energy $\frac{2}{3}$ of that calculated for the compound nucleus. Experimental and simulated (smooth curves) anisotropy ratios ($d^2\sigma_{\parallel}/d^2\sigma_{\perp}$) are also shown in the lower part of (a) and (b).

Thus when we trigger with SST-1 (in-plane correlation) the two wedge detectors sweep the backward hemisphere from $\approx$90–165 deg in the c.m. (A small right-left asymmetry due to kinematic recoil is allowed for in the reaction simulations below.) When we trigger with SST-3 (out-of-plane correlation), the plane of the sweeper detectors is perpendicular to that of the trigger. The SST-2 trigger provides an intermediate position for testing consistency.

Figure 2(a) shows a set of angular correlation data for ^{4}He-^{4}He after transformation into the c.m. system. It is clear that the in-plane correlation is almost isotropic while the out-of-plane correlations have substantial anisotropies. This pattern of anisotropies is a natural consequence of the angular momentum and, in fact, the smooth curves in Fig. 2 were obtained from a reaction simulation[8] as discussed below. This simulation also provides a convenient way to determine angle-integrated multiplicities and cross sections.

Our objectives in this study are threefold. We first examine the evidence concerning the nature and the velocity of the emitting source. Next, we determine the angle-integrated (singles and) coincidence cross sections and separate out the parts arising from the ER chains. Finally, we use the observed energy and angular distributions, in comparison to model calculations, as a probe of the shapes and sizes of the emitting nuclei.

III. PARTICLE-PARTICLE CORRELATIONS

A. The source of the correlated particles

The ER multiplicities strongly suggest that particle-particle coincidences can select out particle evaporation chains that lead to ER's.[7] Nonetheless, it is important to examine in detail, a number of the other signatures which serve as corroborative evidence for this notion.

Figure 2(a) shows a set of angular correlation data for ^{4}He-^{4}He after transformation into the c.m. system. It is clear that the in-plane correlation is almost isotropic while the out-of-plane correlations have substantial anisotropies. This pattern of the anisotropies is a natural consequence of angular momentum alignment, and is consistent with the expected correlations for two particles emitted from a composite nucleus. The smooth curves in Fig. 2(a) were obtained from a reaction simulation for composite-nucleus emission as discussed in a later section. Figure 2(b) shows angular correlations for ^{4}He as triggered by ^{1}H. In this case (for ^{1}H trigger) the in-plane correlation and the out-of-plane correlation have anisotropies that are more similar than those in Fig. 2(a) (for ^{4}He trigger). This effect is particularly emphasized by the correlation anisotropies ($d^2\sigma_{\parallel}/d^2\sigma_{\perp}$) which are shown in the lower part of these figures. The change in the anisotropy pattern with trigger particle is also a natural consequence of evaporation from an equilibrated composite nucleus. Next, the invariant cross section maps for the correlations are examined to establish the velocity of the source of these emissions.

Figures 3 and 4 show in-plane contour maps of the invariant cross sections for ^{4}He in coincidence with ^{4}He

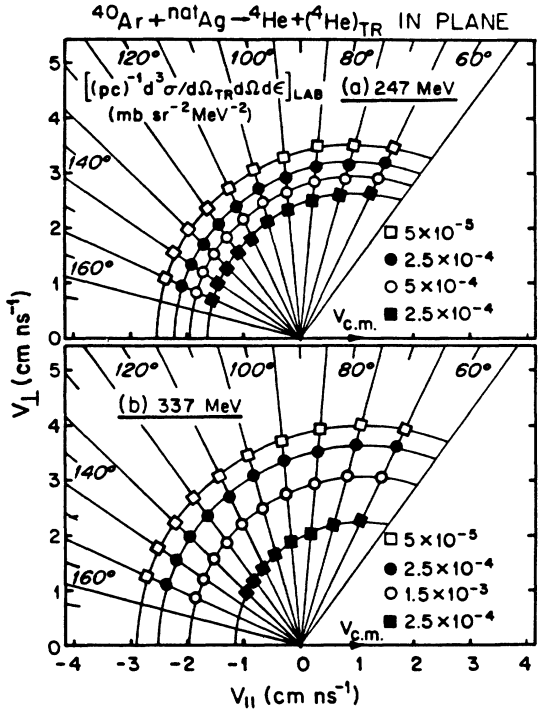

FIG. 3. Contour maps of the invariant cross section for ^{4}He triggered for ^{4}He (in-plane, S-1) for ^{40}Ar beams of (a) 247 MeV and (b) 337 MeV. The circular arcs are centered on $V_{c.m.}$, the velocity of the center of mass. Straight lines are drawn along the laboratory angles as indicated.

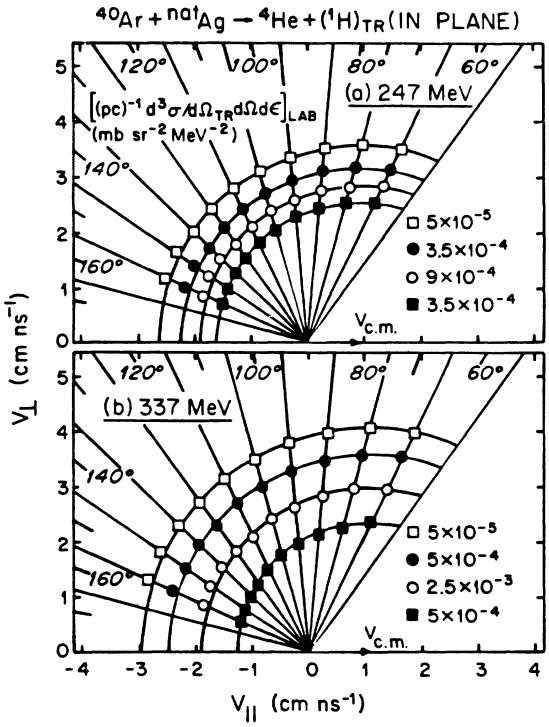

FIG. 4. Contour maps of the invariant cross section for ^{4}He triggered by ^{1}H (in-plane, S-1) for ^{40}Ar beams of (a) 247 MeV and (b) 337 MeV. The circular arcs are centered on $V_{c.m.}$, the velocity of the center of mass. Straight lines are drawn along the laboratory angles as indicated.

and ^{1}H respectively. The circular arcs in these figures are centered on the respective c.m. velocities. In Fig. 3 (^{4}He trigger) these circles describe the results extremely well for both the 247 and 337 MeV ^{40}Ar beams. Small systematic deviations from the circles are observed in Fig. 4 (^{1}H trigger) at the most backward angles. These spin-driven deviations from isotropic emission are another manifestation of the anisotropies in Fig. 2 and are accounted for in the calculations discussed below. A major conclusion from Figs. 3 and 4 is that evaporative emission is indicated from a source moving with the velocity of the center of mass.

Additional information on the source of the emitted particles is also provided by the energy spectra. Figure 5 shows energy spectra for ^{4}He particles as triggered by a second ^{4}He [(a) and (b)] or by ^{1}H [(c) and (d)]. In each frame the upper spectrum was taken with the out-of-plane trigger [S-3 in Fig. 1(a)], and the lower spectrum with the in-plane trigger (S-1). The points at the top of each frame give the ratio $(d^3\sigma_\perp/d^3\sigma_\parallel)$ of the upper spectrum to the lower one; this is the correlation anisotropy versus energy. The smooth curves represent reaction simulation calculations for evaporative emission as described below. The major features are all well described by the simulation (a) the peak positions, (b) the change of the high-energy slope for reactions 337 MeV ^{40}Ar compared to 247 MeV, (c) the nearly constant ratio $(d^3\sigma_\perp/d^3\sigma_\parallel)$ for ^{4}He triggered by ^{1}H, (d) the decrease of $d^3\sigma_\perp/d^3\sigma_\parallel$ with increasing energy for ^{4}He triggered by ^{4}He. The (all-important) input for the simulations will be discussed below; the major point here is that the good fits reinforce confidence in the simulation as a tool to assist in the identification of the source as well as making angle and energy integrations.

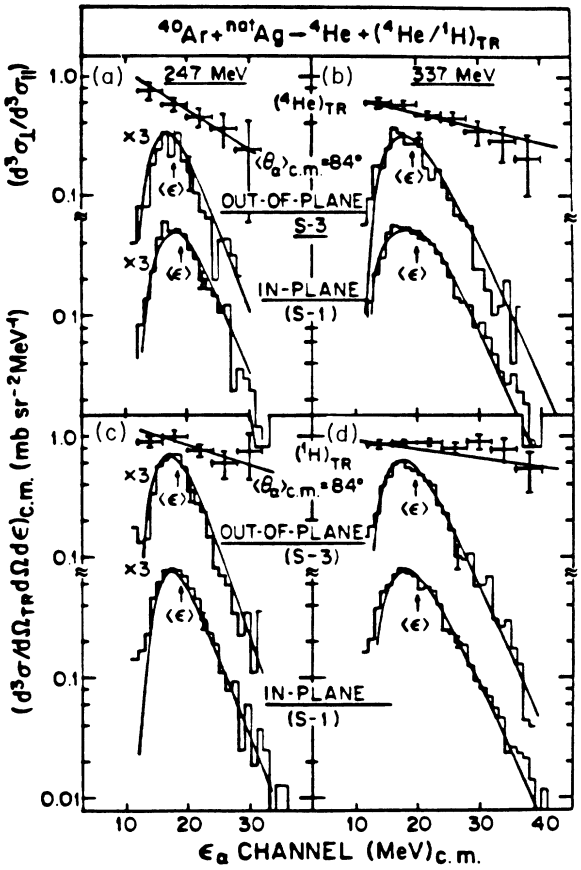

FIG. 5. Energy spectra (c.m.) for ^{4}He detected at $\langle\theta\rangle = 84°$ in coincidence with ^{4}He [(a) and (b)] or ^{1}H [(c) and (d)]. The trigger detector was S-3 (out-of-plane) or S-1 (in-plane) as indicated. The ^{40}Ar beam energy was 247 MeV [(a) and (c)] or 337 MeV [(b) and (d)]. The ratio $d^3\sigma_\perp/d^3\sigma_\parallel$ of out-of-plane to in-plane cross sections is indicated by the points at the top of each frame. The smooth curves were calculated for a spherical emitter with s-wave emission barrier $B = 13.2$ MeV, fractional energy loss of 30% and the same spin zones indicated in Fig. 2.

B. Integrated cross sections and multiplicities

Tables I and II give energy and angle integrated correlation cross sections for 337 and 247 MeV ^{40}Ar respectively. The first block lists inclusive, angle-integrated cross sections for ER, FF, QF, ^{4}He, and ^{1}H. Absolute cross sections from[1] are given for ER, FF, and QF. Our own data[7] for FF and QF are consistent with[1] and were used to fix the relative uncertainties that are given for FF, QF, ^{4}He, and ^{1}H. The second and third blocks list the results from this work for particle-particle double and triple coincidences. The particle-particle, double-coincidence cross sections (σ_{DC}) and associated multiplicities were determined from fits to the data as shown in Figs. 2 and 5. Angle and energy integrations were done with assistance from the reaction simulation code that takes account of recoil effects and angular anisotropies. It was also possible to determine triple coincidence cross sections (σ_{TC}) for 337 MeV ^{40}Ar by requiring that three light particles hit either SST or wedge detectors, or that two light particles register there along with a fragment (FF or QF) in one of the GT's. The double coincidence cross sections have statistical uncertainties of $\approx 5\%$; the triples have rather poor statistical significance with errors of $\approx 20\%$ for particle-particle-particle coincidences and $\approx 30\%$ for fragment-particle-particle coincidences.

In the next section these angle-integrated cross sections are used to draw conclusions about the probability for various particle-emission chains. It is important to point out here that these deductions are limited only by the relative uncertainties of the measurements (i.e., the statistical uncertainties). Absolute errors, from beam integration, target thickness etc., cancel out in these considerations.

IV. PROBABILITIES FOR PRODUCING LIGHT-PARTICLE CHAINS OF VARIOUS SORTS

From a variety of studies it is generally known that ^{1}H and ^{4}He particles are produced in reactions that lead to ER's, FF, and QF with negligible production (into the backward hemisphere) from quasielastic reactions (QER). In this study data have been obtained for singles, coincidences with FF and QF, and particle-particle coincidences. No direct coincidence measurements involving ER's were made, but the particle production cross sec-

TABLE I. Measured cross sections (σ) and multiplicities (M) for 337 MeV ^{40}Ar+^{nat}Ag.

Inclusive angle integrated cross sections (mb).[a]
$\sigma_{ER}=455\pm50$; $\sigma_{FF}=520\pm52$; $\sigma_{QF}=700\pm70$; $\sigma_s^{\alpha}=1223\pm122$; $\sigma_s^{p}=1870\pm187$.
Fragment-particle coincidences[b]

	M_{CE}	σ_{CE} (mb)	M_{FE}	σ_{FE} (mb)	$\sigma_{CE}+\sigma_{FE}$ (mb)
FF-α	0.300±0.030	156±23	0.276±0.028	144±22	300±32
FF-p	0.254±0.025	132±20	0.642±0.064	334±50	466±54
QF-α	0.137±0.014	96±14	0.273±0.027	191±29	286±32
QF-p	0.184±0.018	129±19	0.454±0.045	318±48	447±52

Particle-particle coincidences
Double coincidences[c,d]

	α-α	p-p	p-α
σ_{DC}	1142	2115	1474
M	1.93±0.06	2.13±0.08	0.79±0.06

Triple coincidences[e,f,g]

	α-α-α	p-α-α	α-p-p	p-p-p
σ_{TC}	656	1434	1125	1480
	f-α-α	f-α-p	f-p-α	f-p-p
σ_{TC}	165	320	270	459

[a]Data from Ref. 7 and this work. $\sigma_s^{p,\alpha}=4\pi\int_{\pi/2}^{\pi}(d\sigma/d\Omega)\sin\theta_{c.m.}d\theta_{c.m.}$ The forward peaked component is not included in the integration.
[b]Estimated uncertainties for the multiplicities are ±10%; for the cross sections, errors include those by σ_{FF} and σ_{QF} above.
[c]$\sigma_{DC}=\int\int(d^2\sigma/d\Omega_1 d\Omega_2)d\Omega_1 d\Omega_2$; $M_{\alpha\alpha,pp}=1+\int(d^2\sigma/d\Omega_1 d\Omega_2)/(d\sigma/d\Omega_1)$, and $M_{p\alpha}=\int(d^2\sigma/d\Omega_1 d\Omega_2)/(d\sigma/d\Omega_1)$.
[d]Statistical uncertainties for σ_{DC} are ≈3%.
[e]$\sigma_{TC}=\int\int\int(d^3\sigma/d\Omega_1 d\Omega_2 d\Omega_3)d\Omega_1 d\Omega_2 d\Omega_3$.
[f]Statistical uncertainties for σ_{TC} are ≈20% for particle-particle-particle coincidences, and ≈30% for fragment-particle-particle coincidences.
[g]The value for f-α-p was obtained by detecting an α in the SST's and a proton in the wedge; the converse for f-p-α.

TABLE II. Measured cross sections (σ) and multiplicities (M) for 247 Mev ^{40}Ar+^{nat}Ag.[a]

Inclusive angle integrated cross sections (mb):
$\sigma_{ER}=620\pm80$; $\sigma_{FF}=550\pm55$; $\sigma_{QF}=370\pm37$;
$\sigma_{\alpha}=421\pm42$; $\sigma_{p}=834\pm83$.
Fragment-particle coincidences

	M_{CE}	σ_{CE} (mb)	M_{FE}	σ_{FE} (mb)	$\sigma_{CE}+\sigma_{FE}$ (mb)
FF-α	0.090±0.014	50±10	0.072±0.010	40±8	90±13
FF-p	0.100±0.010	55±11	0.208±0.020	114±12	169±17
QF-α	0.018±0.003	7±1	0.035±0.005	13±3	20±3
QF-p	0.027±0.005	10±2	0.067±0.013	25±5	35±6

Particle-particle coincidences
Double coincidences

	α-α	p-p	p-α
σ_{DC}	265	690	412
M	1.60±0.04	1.77±0.06	0.49±0.04

[a]See footnotes to Table I.

tions in association with the ER's were deduced by taking differences between inclusive cross sections and those obtained from coincidences with FF and QF products. In this section the particle-particle coincidence data (doubles and triples) are used to obtain cross sections for various particle emission chains associated with the production of ER's. The data for 337 MeV ^{40}Ar+^{nat}Ag (Table I) are discussed in detail, and the results are summarized in Table IV. A corresponding analysis of the data for 247 MeV ^{40}Ar (Table II) is summarized in Table V.

A. Average multiplicities

It is instructive to examine a few of the average quantities which are readily obtained from Table I. A total of 1223±122 mb ^{4}He and 1870±187 mb ^{1}H (for 337 MeV ^{40}Ar+^{nat}Ag) are produced from 1675 mb (455 +520+700) of reactions i.e., ≈0.73±0.19 ^{4}He and ≈1.12±0.29 ^{1}H per reaction of any type (ER, FF, and QF). For FF reactions composite evaporation (CE) accounts for only 0.300±0.03 ^{4}He and 0.254±0.025 ^{1}H per reaction, along with 0.276±0.028 ^{4}He and 0.642±0.064 ^{1}H from fragments (FE). Analogous values for QF reactions are 0.137±0.014 ^{4}He and 0.184±0.018 ^{1}H per reaction for composite evaporation (CE) along with 0.273±0.027 ^{4}He and 0.454±0.045 ^{1}H from the target-like fragments (FE). Since the average multiplicities for all reactions are larger than those for either FF or QF, it can be concluded that the ER's are particularly strong particle producers with relatively large multiplicities.

As pointed out in Ref. 7 the average multiplicities for the ER's can be obtained by assigning to the ER's all the evaporative particles which are *not* accounted for by FF or QF reactions. For ^{4}He, the FF and QF reactions account for 586±45 mb of the total alpha production cross section (1223 mb). The remaining 637±177 mb is therefore assigned to the 455±50 mb of ER's which gives 1.40±0.40 ^{4}He per ER. Similarly, there are 1870±187 mb of ^{1}H with 466±54 mb from FF and 447±54 mb from QF; thus, 957±277 mb of ^{1}H are obtained from 455±50 mb of ER's or 2.10±0.60 ^{1}H per ER. (It should be noted that the error bars for the ER multiplicities take account of possible contributions from partially damped reactions as discussed in Ref. 7. These average multiplicities clearly indicate that the mean chain lengths are longer for reactions leading to ER's compared to those for FF or QF.

B. The combined power of singles along with double coincidences

The particle-particle coincidence measurements give more detailed information on these average chain lengths. Using the coincidence cross sections, the average chain length ($M_{\alpha\alpha}$) leading to the observation of one alpha-particle in the trigger detector ($\theta_1 \approx 90°$ in the c.m.) can be evaluated as follows:

$$M_{\alpha\alpha}=1+\left[\int_{\Omega_2} d\Omega_2 \left[\frac{d^2\sigma^{\alpha\alpha}_{DC}}{d\Omega_1 d\Omega_2}\right]\right] \Big/ \left[\frac{d\sigma^{\alpha}_{S}}{d\Omega_1}\right]$$

$$=1.93\pm0.22\ , \qquad (1)$$

where σ^{α}_{S} and $\sigma^{\alpha\alpha}_{DC}$ are the singles and double coincidence cross sections respectively. The symbols Ω_1 and Ω_2 denote solid angles for the trigger and sweeper detectors, respectively. Likewise, an average chain length of 2.13±0.21 is determined for ^{1}H particles in all reactions. It is important to recall here that the inclusive particle cross sections show a smooth variation with detection angle.[7] Hence, it is reasonable to assume that these mean chain lengths, averaged over all values of θ_1, will not differ substantially from the values indicated above for $\theta_1 \approx 90°$. These average chain lengths for ^{4}He and ^{1}H are rather close to the average multiplicities for ER's ($M_\alpha=1.4\pm0.4$; $M_p=2.1\pm0.6$), and are considerably larger than the average multiplicities for FF or QF. This implies a dominant role for the ER's in particle-particle coincidences compared to that for FF [$M_\alpha=0.30$ (CE) or 0.28 (FE); $M_p=0.25$ (CE) or 0.64 (FE)] or for QF [$M_\alpha=0.14$ (CE) or 0.27 (FE); $M_p=0.18$ (CE) or 0.45 (FE)].

Additional information on the production cross sections and chain lengths can be obtained by focusing on the singles and the double coincidence measurements for a selected class of reactions. Consider the production of a set of products (A) which, on average, emit a sequence of $\langle n_\alpha \rangle$ ^{4}He or $\langle m_p \rangle$ ^{1}H particles. Let σ_A be the cross section for producing this set; then the ^{4}He and ^{1}H singles cross sections [$\sigma^{\alpha}_{S}(A)$ and $\sigma^{p}_{S}(A)$] from this set can be written as

$$\sigma^{\alpha}_{S}(A)=\sigma_{A_\alpha}\langle n_\alpha \rangle, \quad \sigma^{p}_{S}(A)=\sigma_{A_p}\langle m_p \rangle\ , \qquad (2)$$

where σ_{A_α} and σ_{A_p} are average subset cross sections for the products which emit ^{4}He and ^{1}H respectively. The fact that the subset cross sections (σ_{A_p} and σ_{A_α}) in Eq. (2) may be different from σ_A allows the possibility that some ER's may not emit ^{4}He or ^{1}H and that the overlap between ^{4}He and ^{1}H emitters may not necessarily be complete.

For indistinguishable particles (e.g., α-α or p-p) the double coincidence cross sections can be evaluated from the following expressions:

$$\sigma^{\alpha\alpha}_{DC}(A)=\sigma_{A_\alpha}\langle n_\alpha(n_\alpha-1)\rangle\ ,$$
$$\sigma^{pp}_{DC}(A)=\sigma_{A_p}\langle m_p(m_p-1)\rangle, \quad \text{for } n,m>1\ , \qquad (3)$$

while for distinguishable particles (e.g., p-α)

$$\sigma^{p\alpha}_{DC}(A)=\sigma_{A_{p\alpha}}\langle m_p \rangle\langle n_\alpha \rangle\ . \qquad (4)$$

Here $\sigma_{A_{p\alpha}}$ denotes the average overlap between σ_{A_p} and σ_{A_α}, i.e., the subset cross section for products which on average emit n ^{4}He and m ^{1}H particles. (The multiplicity coefficients in Eqs. (3) and (4) are derived from the combinatorial factors P_k [$P_k=n(n-1)(n-2)\cdots(n-k)$.]) In Eqs. (2)–(4) it has been assumed that the average chain lengths ($\langle n_\alpha \rangle$ or $\langle m_p \rangle$) are associated with average subset cross sections (σ_{A_α}, σ_{A_p}, and $\sigma_{A_{p\alpha}}$). It is important to note, however, that this is not a necessary assumption for the determination of the average chain lengths: the average multiplicity or chain length can be determined from the equation

$$\langle M\rangle = 1+\left\{\int_{\Omega_2}\int_{\Omega_1} d\Omega_2 d\Omega_1\left[\frac{d^2\sigma_{\rm DC}(A)}{d\Omega_1 d\Omega_2}\right]\right\}\Big/\left\{\int_{\Omega_1} d\Omega_1\left[\frac{d\sigma_{\rm S}(A)}{d\Omega_1}\right]\right\}, \tag{5}$$

which is independent of the subset cross sections.

From Eqs. (2)–(4) it is clear that one can obtain values for the average subset cross sections (σ_{A_α}, σ_{A_p}, and $\sigma_{A_{p\alpha}}$) and the average multiplicities ($\langle m_p\rangle$ or $\langle n_\alpha\rangle$) if the singles and double coincidence cross sections (σ_S^α, σ_S^p, $\sigma_{DC}^{\alpha\alpha}$, and σ_{DC}^{pp}) can be fixed for a certain specified set of reactions. Since it has been shown that the coincidence cross sections are dominated by the ER's it is natural to focus on these ER products as the specified set of choice.

The singles cross sections for the ER's were determined earlier;

$$\sigma_S^\alpha(\mathrm{ER})=637\pm177\ \mathrm{mb},\quad \sigma_S^p(\mathrm{ER})=957\pm277\ \mathrm{mb}\ . \tag{6}$$

Similarly, the double coincidence cross sections

$$\sigma_{\rm DC}=\int_{\Omega_1}\int_{\Omega_2}(d^2\sigma_{\rm DC}/d\Omega_1 d\Omega_2)d\Omega_1 d\Omega_2 \tag{7}$$

have been measured as follows:

$$\sigma_{DC}^{\alpha\alpha}=1142\pm57\ \mathrm{mb},\quad \sigma_{DC}^{pp}=2115\pm64\ \mathrm{mb}$$

and

$$\sigma_{DC}^{p\alpha}=1474\pm59\ \mathrm{mb}\ . \tag{8}$$

These overall double coincidence cross sections undoubtedly have some contribution from FF and QF reactions. These contributions must be subtracted in order to get both σ_S(ER) and σ_{DC}(ER) for the same set, namely the ER's. The measured fragment-particle-particle cross sections ($\sigma_{TC}^{f\alpha\alpha}$, σ_{TC}^{fpp}, and $\sigma_{TC}^{fp\alpha}$) shown in Table I, provide the most direct route for such subtractions. However, as their statistical significance is rather weak, estimates were also made from the FF and QF double coincidence multiplicities.

Table III summarizes the estimated as well as the experimental cross sections for producing two-particle chains in FF or QF reactions. The estimated values for both beam energies were determined by assuming independent emission probabilities for CE and FE. In other words, it was assumed that the decisions for FE decay are made after complete memory loss of earlier decisions made for CE decay. Additionally, chain lengths of three or more particles from FF or QF reactions were neglected. This neglect is justified by the very small average multiplicities obtained for these reactions. The algebraic details of the estimates are given in the Appendix. Despite relatively large experimental uncertainties, Table III indicates that there is good agreement between the experimental and the estimated cross sections. This result strengthens the validity of the assumption employed in the estimates. (See Appendix.)

TABLE III. Cross sections (σ_{TC}) for two particle chains in FF and QF reactions. [Angle integrated cross sections for two particles (α or p) in coincidence with a fissionlike fragment (f) as indicated].

	337 MeV ^{40}Ar+$^{\rm nat}$Ag	
	Estimated cross sections (mb)[a]	Measured cross sections (mb)
$\sigma_{TC}^{f\alpha\alpha}$	158	165±50
$\sigma_{TC}^{fp\alpha}$	382	295±81
σ_{TC}^{fpp}	394	459±138

[a]Details of these estimates are given in the Appendix.

The results in Table III can now be used to correct the double coincidence ^{4}He-^{4}He, ^{1}H-^{1}H, and ^{4}He-^{1}H cross sections. Thus for the set of ER reactions

$$\sigma_S^\alpha(\mathrm{ER})=637\pm177\ \mathrm{mb}=\sigma_{A_\alpha}\langle n_\alpha\rangle\ , \tag{9}$$

and

$$\sigma_{DC}^{\alpha\alpha}(\mathrm{ER})=984\pm70\ \mathrm{mb}=\sigma_{A_\alpha}\langle n_\alpha(n_\alpha-1)\rangle\ . \tag{10}$$

These equations can be solved for σ_{A_α} and $\langle n_\alpha\rangle$ if we make the approximation that the distribution about $\langle n_\alpha\rangle$ is very narrow; i.e., that all reactions emit the average number of alpha particles. (We will relax this approximation later.) The solution of Eqs. (9) and (10) gives values of 2.54±0.73 and 251±73 mb for $\langle n_\alpha\rangle$ and σ_{A_α}, respectively. Similarly, for the protons

$$\sigma_S^p(\mathrm{ER})=957\pm277\ \mathrm{mb}=\sigma_{A_p}\langle m_p\rangle\ , \tag{11}$$

and

$$\sigma_{DC}^{pp}(\mathrm{ER})=1721\pm152\ \mathrm{mb}=\sigma_{A_p}\langle m_p(m_p-1)\rangle\ . \tag{12}$$

The solution of these equations gives values of 2.80±0.80 and 342±97 mb for $\langle m_p\rangle$ and σ_{A_p}, respectively.

It is interesting to compare these average multiplicities and subset cross sections with those obtained from the singles data for the ER's:

$$\sigma_{\rm ER}=455\ \mathrm{mb}\ , \tag{13}$$

$$M_\alpha=\langle n_\alpha\rangle=1.4\pm0.4\ , \tag{14}$$

$$M_p=\langle m_p\rangle=2.1\pm0.6\ . \tag{15}$$

This comparison indicates that among the 455 mb of ER reactions, there is a subset of $\approx$251 mb that emits $\approx$2.5 α particles on average (much more than the overall ER average of 1.4). Similarly, for the protons there is a subset of $\approx$342 mb that emits $\approx$2.8 protons (somewhat more than the ER average of 2.1). It is also noteworthy that the sum of these two subset cross sections (σ_{A_p} and σ_{A_α}) *exceeds* $\sigma_{\rm ER}$. This result implies that there is an overlap between the subset cross sections which accounts for ^{4}He and ^{1}H emission. In the next subsection the extent as well as the implications of such an overlap are investigated.

C. "Overlap" of ^{1}H and ^{4}He production

Another important double coincidence measurement is the proton-alpha correlation cross section (i.e., $\sigma_{DC}^{p\alpha}$). The measured value for all reactions as reported in Table I is 1474±59 mb. After correcting for the contributions from FF and QF reactions, the value of $\sigma_{DC}^{p\alpha}$(ER) is 1092±120 mb. This correlation cross section from the ER's, imposes a very important constraint, namely the overlap of σ_{A_α} (251 mb) with σ_{A_p} (342 mb).

The extent of this overlap can be determined from Eq. (4) if the previously calculated chain lengths for ^{1}H and ^{4}He ($\langle m_p \rangle$ and $\langle n_\alpha \rangle$) are employed. After appropriate substitutions, Eq. (4) can be written as

$$\sigma_{DC}^{p\alpha}(\mathrm{ER}) = 1092 \text{ mb} = \sigma_{A_{p\alpha}} \langle m_p \rangle \langle n_\alpha \rangle ,$$
$$= \sigma_{A_{p\alpha}} (2.5)(2.8) , \quad (16)$$

which gives a value of 154±60 mb for $\sigma_{A_{p\alpha}}$. This overlap cross section is substantially less than σ_{A_α} or σ_{A_p}. Consequently, it can be concluded that a large number of reactions occur in which ^{1}H or ^{4}He are produced but not both. In fact the result indicates that, on average, *less* than 50% of the proton emitters also emit alpha particles in the same event.

The apparently small overlap between ^{1}H and ^{4}He emitters is consistent with qualitative aspects of statistical model predictions.[17,11–13] Standard evaporation models predict that α-particle evaporation increases with increasing spin of the emitter while the proton emission decreases. Thus, it is reasonable to assume that the set of proton-chain reactions is biased toward lower spins and the set of alpha-chain reactions is biased toward higher spins. The overlap cross section, of course, does not allow one to attribute the alphas to the higher spin zone. However, this attribution can be confirmed by reference to the angular correlations for ^{4}He in coincidence with ^{1,2,3}H and ^{4}He as discussed below.

The consistency of the subset cross sections and chain lengths determined thus far, can be tested against the observed value of σ_{ER}. This follows naturally from the fact that the sum of the subset cross sections, after correcting for their overlap, can*not* exceed σ_{ER}. The total cross section for all ^{4}He and ^{1}H subsets (σ_A) is given by

$$\sigma_A = \sigma_{A_\alpha} + \sigma_{A_p} - \sigma_{A_{p\alpha}}$$
$$= (251 + 392 - 154) \text{ mb} = 439 \text{ mb} . \quad (17)$$

This value of σ_A is essentially identical to the ER cross section of 455 mb. Therefore, the inferred values of the subset cross sections (σ_{A_α} and σ_{A_p}) do fit inside the allowed total cross section for ER's.

D. Combined use of singles along with double and triple coincidences

In the foregoing analysis, the triple coincidence cross sections (for one fragment in coincidence with two particles) were used to correct the double coincidence particle-particle cross sections for FF and QF contributions. By contrast, the triple-particle coincidence cross sections provide additional information on the chain lengths, and subset cross sections. In analogy to Eqs. (2) and (3), the triple-coincidence cross sections (σ_{TC}) for indistinguishable particles can be written as

$$\sigma_{TC}^{\alpha\alpha\alpha}(A) = \sigma_{A'_\alpha} \langle n_\alpha (n_\alpha - 1)(n_\alpha - 2) \rangle , \quad (18)$$

and

$$\sigma_{TC}^{ppp}(A) = \sigma_{A'_p} \langle m_p (m_p - 1)(m_p - 2) \rangle , \quad (19)$$

for alphas and protons respectively. Similarly, for distinguishable particles (e.g., p$\alpha\alpha$) one can write

$$\sigma_{TC}^{p\alpha\alpha}(A) = \sigma_{A'_{p\alpha}} \langle m_p \rangle \langle n_\alpha (n_\alpha - 1) \rangle . \quad (20)$$

Equations (18)–(20) can be used to determine chain lengths and subset cross sections in an analysis similar to that of the previous subsection. However, the problem associated with the use of these equations is the different averaging implicit in each of them. A better approach is to use a set of equations that considers the sum of the contributions from the respective chains. Thus for ^{4}He emission from a given set of products (e.g., the ER's), these equations can be written as

$$\sigma_S^\alpha(\mathrm{ER}) = \sum_{n=1}^{k} \sigma_{A_\alpha^n}(n_\alpha) , \quad (21)$$

$$\sigma_{DC}^{\alpha\alpha}(\mathrm{ER}) = \sum_{n=2}^{k} \sigma_{A_\alpha^n}(n_\alpha)(n_\alpha - 1) , \quad (22)$$

$$\sigma_{TC}^{\alpha\alpha\alpha}(\mathrm{ER}) = \sum_{n=3}^{k} \sigma_{A_\alpha^n}(n_\alpha)(n_\alpha - 1)(n_\alpha - 2) . \quad (23)$$

Here $\sigma_{A_\alpha^n}$ and $\sigma_{A_\alpha^m}$ are subset cross sections (ER) associated with emission chains of length n or m, respectively. If the three-particle chains associated with QF and FF reactions are assumed to be negligible, and k is set to the value 3, then the following equations are obtained for 337 MeV ^{40}Ar+^{nat}Ag:

$$\sigma_{TC}^{\alpha\alpha\alpha}(\mathrm{ER}) = 6\sigma_{A_\alpha^3} = 656 \text{ mb} , \quad (24)$$

$$\sigma_{DC}^{\alpha\alpha}(\mathrm{ER}) = 2\sigma_{A_\alpha^2} + 6\sigma_{A_\alpha^3} = 984 \text{ mb} , \quad (25)$$

$$\sigma_S^\alpha(\mathrm{ER}) = \sigma_{A_\alpha^1} + 2\sigma_{A_\alpha^2} + 3\sigma_{A_\alpha^3} = 637 \text{ mb} . \quad (26)$$

The solution of these equations gives

$$\sigma_{A_\alpha^3} = 109 \pm 22 \text{ mb} ,$$
$$\sigma_{A_\alpha^2} = 164 \pm 40 \text{ mb} ,$$
$$\sigma_{A_\alpha^1} = -18 \pm 142 \text{ mb} .$$

Clearly, one cannot have a negative cross section, so it must be concluded that $\sigma_{A_\alpha^1}$ is simply very small.

For the emission of proton chains, a similar analysis has been carried out to obtain the following subset cross sections:

$$\sigma_{A_p^3} = 247 \pm 49 \text{ mb} ,$$
$$\sigma_{A_p^2} = 121 \pm 170 \text{ mb} ,$$
$$\sigma_{A_p^1} = -26 \pm 374 \text{ mb} .$$

The uncertainties on $\sigma_{A_p^m}$ for protons are larger than those for the alphas due to the subtraction of large numbers. Nevertheless, the general pattern is clear. A comparison of the $\sigma_{A_\alpha^n}$ and $\sigma_{A_p^m}$ values given above indicates that $\sigma_{A_\alpha^3} > \sigma_{A_\alpha^1}$ and $\sigma_{A_p^3} > \sigma_{A_p^1}$. It is therefore important to investigate possible contributions from $n=4$ and $m=4$ chains. Using Eqs. (21)–(23), these contributions can be estimated by setting $k=4$ and assuming that $\sigma_{A_{\alpha,p}^1}=0$. This attack leads to essentially the same values for $\sigma_{A_{\alpha,p}^2}$ and $\sigma_{A_{\alpha,p}^3}$ with $\sigma_{A_{\alpha,p}^4} \approx 0$. These results indicate that chain lengths ≥ 4 are rare and further suggest that the results above (for $k=3$) give a reasonable set of values for $\sigma_{A_\alpha^n}$ and $\sigma_{A_p^m}$ (albeit with large error bars as stated).

The triple-particle coincidence cross sections $\sigma_{TC}^{p\alpha\alpha}$ and $\sigma_{TC}^{\alpha pp}$ provide additional qualitative insight on the overlap of ^{1}H and ^{4}He production. The values reported in Table I for $\sigma_{TC}^{p\alpha\alpha}$ and $\sigma_{TC}^{\alpha pp}$ are, respectively, 1434±286 mb and 1125±225 mb. These relatively small cross sections can also test the notion that the overlap between the subset cross sections for ^{1}H and ^{4}He production ($\sigma_{A_\alpha^{2,3}}$ and $\sigma_{A_p^{2,3}}$) is incomplete; a complete overlap between $\sigma_{A_\alpha^{2,3}}$ and $\sigma_{A_p^{2,3}}$ would give

$$\sigma_{TC}^{p\alpha\alpha}(\mathrm{ER}) = \sigma_{A_\alpha}\langle m_p\rangle\langle n_\alpha\rangle\langle n_\alpha - 1\rangle \quad (27)$$

$$= 273(2.4)(1.4)(2.5) = 2477 \text{ mb} , \quad (28)$$

and

$$\sigma_{TC}^{\alpha pp}(\mathrm{ER}) = \sigma_{A_\alpha}\langle n_\alpha\rangle\langle m_p\rangle\langle m_p - 1\rangle \quad (29)$$

$$= 273(2.4)(2.5)(1.5) = 3007 \text{ mb} , \quad (30)$$

where $\langle n_\alpha\rangle$ and $\langle m_p\rangle$ are the average (weighted) multiplicities associated with $\sigma_{A_\alpha^{2,3}}$ and $\sigma_{A_p^{2,3}}$ respectively; σ_{A_α} denotes the sum of $\sigma_{A_\alpha^2}$ and $\sigma_{A_\alpha^3}$.

A reasonable way to account for the unacceptably large values from Eqs. (27)–(30) is to suppose that the average proton multiplicity m_p is a decreasing function of the spin of the composite nucleus, and the converse for the average alpha multiplicity n_α (for the spin zone of the ER's). Such a path can be followed in more detail as follows. Let n_α increase with increasing spin while m_p decreases with increasing spin, both according to the sharp cutoff approximation. Then the spin distribution for the ER's (455 mb) can be divided into appropriate segments according to the values for $\sigma_{A_\alpha^{0,1,2,3}}$ and $\sigma_{A_p^{0,1,2,3}}$. Using this prescription, the following assignments can be made in order of increasing spin zone:

$$\sigma_{A_\alpha^0} = 182 \text{ mb} \quad (0 \leq l_0 \leq 44) , \qquad \sigma_{A_p^3} = 247 \text{ mb} \quad (0 \leq l_0 \leq 52) , \quad (31)$$

$$\sigma_{A_\alpha^1} = 0 \text{ mb} , \qquad \sigma_{A_p^2} = 121 \text{ mb} \quad (52 < l_0 \leq 63) , \quad (32)$$

$$\sigma_{A_\alpha^2} = 164 \text{ mb} \quad (44 < l_0 \leq 61) , \qquad \sigma_{A_p^1} = 0 \text{ mb} , \quad (33)$$

$$\sigma_{A_\alpha^3} = 109 \text{ mb} \quad (61 < l_0 \leq 70) , \qquad \sigma_{A_p^0} = 87 \text{ mb} \quad (63 < l_0 \leq 70) . \quad (34)$$

Folding these assignments together, one can estimate values for $\sigma_{TC}^{p\alpha\alpha}(\mathrm{ER})$ and $\sigma_{TC}^{\alpha pp}(\mathrm{ER})$ by summing the separate contributions from the ER chains that produce both ^{1}H and ^{4}He.

$$\sigma_{TC}^{p\alpha\alpha}(\mathrm{ER}) = \sum_m^k \sum_n^k \sigma_{A_{p\alpha}^{n+m}}(m_p)(n_\alpha)(n_\alpha - 1) , \quad (35)$$

$$\sigma_{TC}^{\alpha pp}(\mathrm{ER}) = \sum_n^k \sum_m^k \sigma_{A_{p\alpha}^{n+m}}(n_\alpha)(m_p)(m_p - 1) , \quad (36)$$

where $\sigma_{A_{p\alpha}^{n+m}}$ is the subset cross section (ER) associated with the production of n alpha-particles and m protons. Substituting the previously assigned cross sections [Eqs. (31)–(34)] into Eqs. (35) and (36), one obtains

$$\sigma_{TC}^{p\alpha\alpha}(\mathrm{ER}) = 65(3)(2) + 99(2)(2) + 22(2)(3)(2)$$

$$= 1050 \text{ mb} , \quad (37)$$

and

$$\sigma_{TC}^{\alpha pp}(\mathrm{ER}) = 65(2)(3)(2) + 99(2)(2) + 22(2)(3)$$

$$= 1308 \text{ mb} . \quad (38)$$

These calculated cross sections are much closer to the experimental values. Hence, they give strength to the idea that the variation of n_α and m_p with spin are indeed in opposite directions. It should be reemphasized that the cross section argument given here does not actually allow one to attribute the alphas to the higher spin zones. However, as pointed out earlier, this attribution can be confirmed by reference to the angular distributions for ^{4}He in coincidence with ^{1,2,3}H and ^{4}He.

The same kind of analysis has also been performed for 247 MeV ^{40}Ar+^{nat}Ag with the assumption that there are negligible amounts of $\alpha\alpha\alpha$ or ppp chains. The resulting values of $\sigma_{A_\alpha^1}$, $\sigma_{A_\alpha^2}$, $\sigma_{A_p^1}$, and $\sigma_{A_p^2}$ are given in Table V. The combined results of Tables IV and V clearly demonstrate the importance of evaporation chains with multiple charged particle emission.

E. Use of the Poisson distribution

Another approach to the analysis of these cross sections can be found in the use of the Poisson distribution. If the emission for a given particle is constant for a long evaporation chain, then one expects to observe a Poisson distribution P_x of chain lengths (x)

TABLE IV. Summary of the cross sections (σ) associated with the evaporation residues (ER). [σ_{DC} and σ_S denote singles and double coincidence particle cross sections as indicated. The subset cross sections (ER) associated with the production of m protons, n alphas, and m protons $+n$ alphas are denoted by $\sigma_{A_p^m}$, $\sigma_{A_\alpha^n}$, and $\sigma_{A_{p\alpha}^{m+n}}$ respectively (see text).]

337 MeV ^{40}Ar+^{nat}Ag
$\sigma_{ER}=455\pm50$ mb
$\sigma_S^{\alpha}(ER)=637\pm177$ mb with $1.4\pm0.4\alpha$ per ER
$\sigma_S^{p}(ER)=957\pm277$ mb with 2.1 ± 0.6 p per ER
$\sigma_{DC}^{\alpha\alpha}(ER)=984\pm70$ mb with $\sigma_{A_\alpha}=251\pm73$ mb and $\langle n_\alpha\rangle=2.54\pm0.73$
$\sigma_{DC}^{pp}(ER)=1721\pm152$ mb with $\sigma_{A_p}=342\pm97$ mb and $\langle m_p\rangle=2.8\pm0.80$
$\sigma_{DC}^{p\alpha}(ER)=1092\pm120$ mb with $\sigma_{A_{p\alpha}}=154\pm60$ mb
$\sigma_{A_\alpha}+\sigma_{A_p}-\sigma_{A_{p\alpha}}=439$ mb
$\sigma_{A_\alpha^1}=-18\pm142$ mb; $\sigma_{A_\alpha^2}=164\pm40$ mb; $\sigma_{A_\alpha^3}=109\pm22$ mb
$\sigma_{A_p^1}=-26\pm374$ mb; $\sigma_{A_p^2}=121\pm170$ mb; $\sigma_{A_p^3}=247\pm49$ mb
$\sigma_{A_{p\alpha}^{3+2}}\approx65$ mb; $\sigma_{A_{p\alpha}^{2+2}}\approx99$ mb; $\sigma_{A_{p\alpha}^{2+3}}\approx22$ mb

$$P_x=\langle x\rangle^x\frac{\exp-\langle x\rangle}{x!}\ . \tag{39}$$

Here the excitation energy limits the evaporation chain to about a dozen particles so we can expect the need for a requirement to truncate this distribution. In addition, the physics of the particle emission probabilities may apply an additional limit on the chain length. Nevertheless, one might expect the ^{4}He (or ^{1}H) emission probabilities to be roughly constant for several emission steps, and thus it is attractive to use Eq. (39) as an approximate basis for characterizing the ^{4}He (or ^{1}H) chain lengths.

We begin by setting $\langle x\rangle$ to σ_S/σ_{ER} i.e., $\langle x_\alpha\rangle=1.4$ and $\langle x_p\rangle=2.1$ for 337 MeV ^{40}Ar. Then we can list the "full" Poisson distributions as given in Table VI. From Eqs. (21)–(23) we calculate the values of σ_S, σ_{DC}, and σ_{TC} as given below the distribution. The calculated values of σ_{TC} are greater than the experimental values; thus, we see the signature for the expected need to truncate the distribution. The "cut" distributions in Table VI were truncated in such a way as to obtain an approximate accord with each of the experimental values of σ_S, σ_{DC}, and σ_{TC}.

These "cut" distributions can be viewed as alternatives to the values of $\sigma_{A^1},\sigma_{A^2}\cdots$ that were obtained in the last section. The presence in these distributions of long chain lengths ($\sigma_{A^4},\sigma_{A^5}$) is offset by an increase of σ_{A^1} compared to the values in Table IV. The regularity of these modified Poisson distributions is intuitively attractive and similar to what one expects from a multistep evaporation calculation. The comparison of these results to such a detailed calculation leads to a number of considerations beyond the scope of this study. Such comparisons will, however, be given in a future publication.[18]

TABLE V. Summary of the cross sections (σ) associated with the evaporation residues (ER). [σ_{DC} and σ_S denote singles and double coincidence particle cross sections as indicated. The subset cross sections (ER) associated with the production of n alphas and m protons are denoted by $\sigma_{A_\alpha^n}$ and $\sigma_{A_p^m}$ respectively (see text).]

247 MeV ^{40}Ar+^{nat}Ag
$\sigma_{ER}=620\pm80$ mb
$\sigma_S^{\alpha}(ER)=311\pm50$ mb with $0.501\pm0.101\alpha$ per ER
$\sigma_S^{p}(ER)=630\pm88$ mb with 1.02 ± 0.20 p per ER
$\sigma_{DC}^{\alpha\alpha}(ER)=255\pm26$ mb with $\sigma_{A_\alpha}=170\pm52$ mb and $\langle n_\alpha\rangle=1.8\pm0.54$
$\sigma_{DC}^{pp}(ER)=654\pm75$ mb with $\sigma_{A_p}=309\pm96$ mb and $\langle m_p\rangle=2.0\pm0.61$
$\sigma_{DC}^{p\alpha}(ER)=389\pm40$ mb with $\sigma_{A_{p\alpha}}=108\pm38$ mb
$\sigma_{A_\alpha}+\sigma_{A_p}-\sigma_{A_{p\alpha}}=371$ mb
$\sigma_{A_\alpha^1}=56\pm45$ mb; $\sigma_{A_\alpha^2}=128\pm13$ mb
$\sigma_{A_p^1}=-24\pm90$ mb; $\sigma_{A_p^2}=327\pm35$ mb

TABLE VI. Poisson distributions of chain lengths compared to the observed cross sections. [$\sigma_0, \sigma_1, \ldots, \sigma_n$ denotes the cross sections for a given chain length. σ_S, σ_{DC}, and σ_{TC} denote singles, doubles, and triple coincidence cross sections as calculated from the distributions (block 2) or as observed experimentally (block 3).]

	337 MeV ^{40}Ar+^{nat}Ag			
	^{4}He		^{1}H	
	$M_\alpha = 1.4$		$M_p = 2.1$	
σ_n	full[a]	cut[b]	full[a]	cut[b]
σ_0	112	112	56	56
σ_1	157	157	117	117
σ_2	110	110	123	123
σ_3	51	51	86	86
σ_4	18	18	45	45
σ_5	5	2	19	3
σ_6	1	0	7	0
σ_7	0	0	2	0
σ_8	0	0	0	0
σ_9	0	0	0	0
σ_S	632	612	952	816
σ_{DC}	872	782	1976	1362
σ_{TC}	1158	858	3996	1776
	Experimental values			
σ_S	637		957	
σ_{DC}	984		1721	
σ_{TC}	656		1480	

[a]This is the complete Poisson distribution.
[b]This Poisson distribution has been truncated between σ_4 and σ_5.

V. RELATION OF STATISTICAL MODEL TO EXPERIMENTAL RESULTS

In the foregoing discussions, the mean velocity of the emitting nuclei was shown to be essentially equal to that of the c.m. Similarly, the particle-particle coincidence cross sections were found to be dominated by ER chains. In fact, an inspection of Tables I and II indicates that for 337 (247) MeV ^{40}Ar reactions, over 80% (90%) of these coincidences are derived from the ER's. Thus, the notion that the particle-particle coincidences are derived from complete-fusion composite nuclei can be accepted.

In this section, the simulated energy and angular correlations from these emitters are compared to the corresponding experimental correlations. Briefly, the results from these comparisons can be summarized as follows: (1) The detailed features of the angular correlations are very well accounted for by the statistical model calculations. (2) The energy distributions for the light charged particles can also be accounted for, but only if quite low evaporation barriers (relative to empirical fusion barriers) are employed in the calculations. (3) Calculations performed for particle emission from a deformed emitter indicate that deformation is probably not the cause of the rather low particle energies observed. (4) In fact, no reasonable deformation appears to be sufficient for an adequate description of the energy spectra for the protons. For the alpha particles, the extent of the deformation required seems to be unimaginable for an emitter that does not subsequently undergo fission. The details of these findings are addressed in the next two subsections.

A. Relation to angular correlations

The measured cross sections for the ER's indicate spin zones $0-70\hbar$ and $0-68\hbar$, respectively, for reactions of 337 MeV and 247 MeV ^{40}Ar.[1] One set of reaction simulation calculations was made with the assumption that composite nuclei of all spins contribute equal multiplicities for the emission chains ^{4}He-^{4}He and ^{1}H-^{4}He. These calculated angular correlations, for emission from a spherical nucleus, are compared to the data in Fig. 6; they are generally quite acceptable except for a small underestimate of the out-of-plane anisotropy for ^{4}He-^{4}He. In Sec. IV above, it was shown that there is probably a spin fractionation that separates the spin zone of predominant ^{4}He emission from that for predominant ^{1}H emission. A general feature of the statistical model is that ^{4}He emission is favored for higher spins compared to ^{1}H emission. Therefore, in a second set of simulations, a spin zone of $35-70\hbar$ was used for the ^{4}He-^{4}He chains; this gives excellent fits as shown in Fig. 2(a). For the ^{1}H-

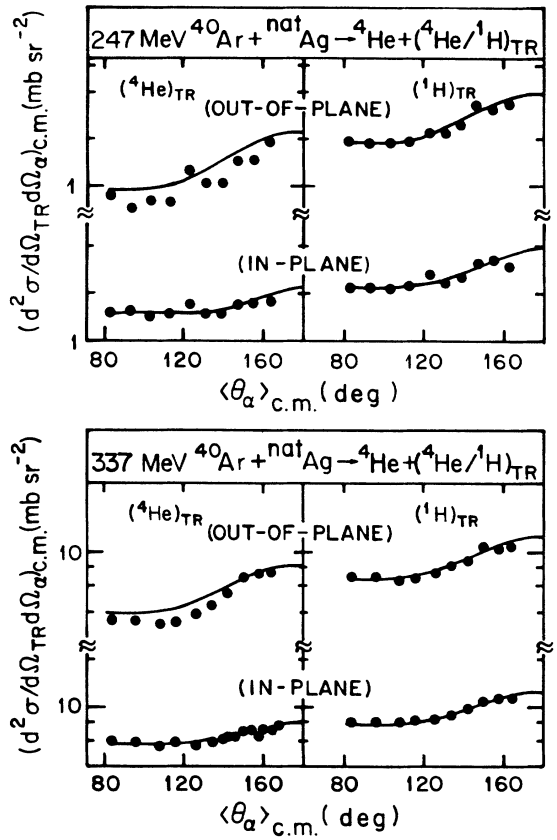

FIG. 6. Angular correlations for ^{4}He in coincidence with ^{4}He or ^{1}H trigger particles. Out-of-plane triggers were S-3 and in-plane were S-1. Curves are calculated for evaporation from spherical emitters with initial excitation $\frac{2}{3}$ of that calculated for the c.m. and spin zones of $0 < J < 70\hbar$.

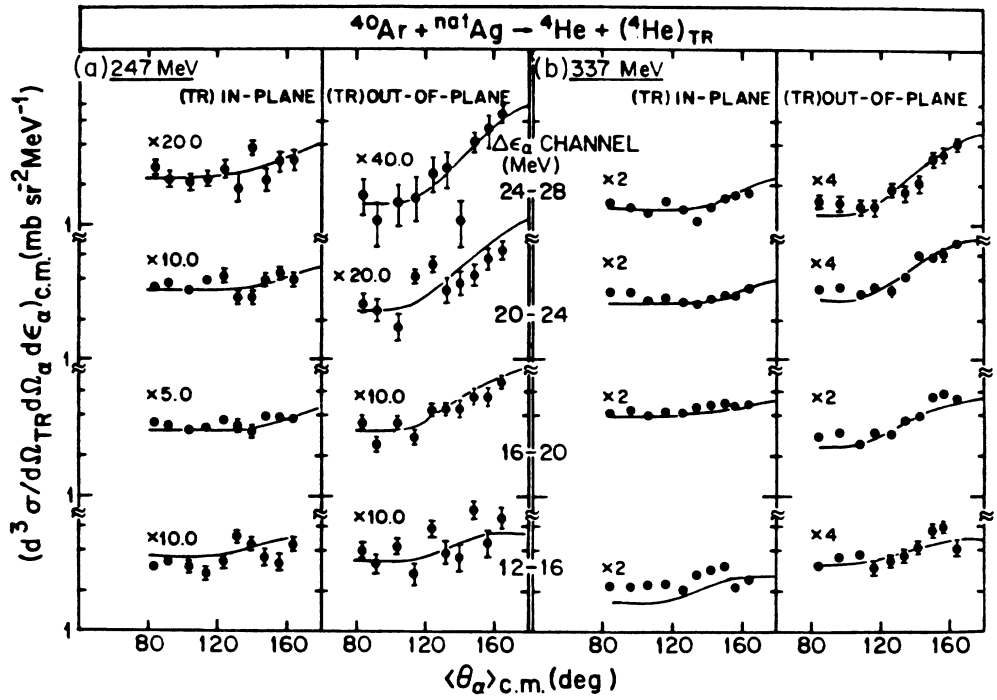

FIG. 7. Measured ^{4}He-^{4}He correlation distributions (in the c.m.) as a function of the energy bin ΔE_α. Solid curves were calculated as described in Fig. 2(a) i.e., $35 < J < l_{ER}$ and $\langle E^* \rangle = \frac{2}{3} E_{CN}$.

^{4}He correlations [Figs. 2(b) and 6], a J_{rms} value of $50\hbar$ gives a very good fit. (Note that this J_{rms} value is the root-mean-square value for the spin zone which characterizes the ER's.)

It is clear that a spherical emitter can account for the overall angular distributions as shown in Figs. 2 and 6. However, much more detailed tests of these angular distributions are provided in Figs. 7 and 8. In these figures, energy cuts on the exit-channel energy for both 247 and 337 MeV ^{40}Ar were made for both the ^{4}He trigger (Fig. 7) and the ^{1}H trigger (Fig. 8). These energy cuts were made subsequent to fitting the energy spectra as illustrated in

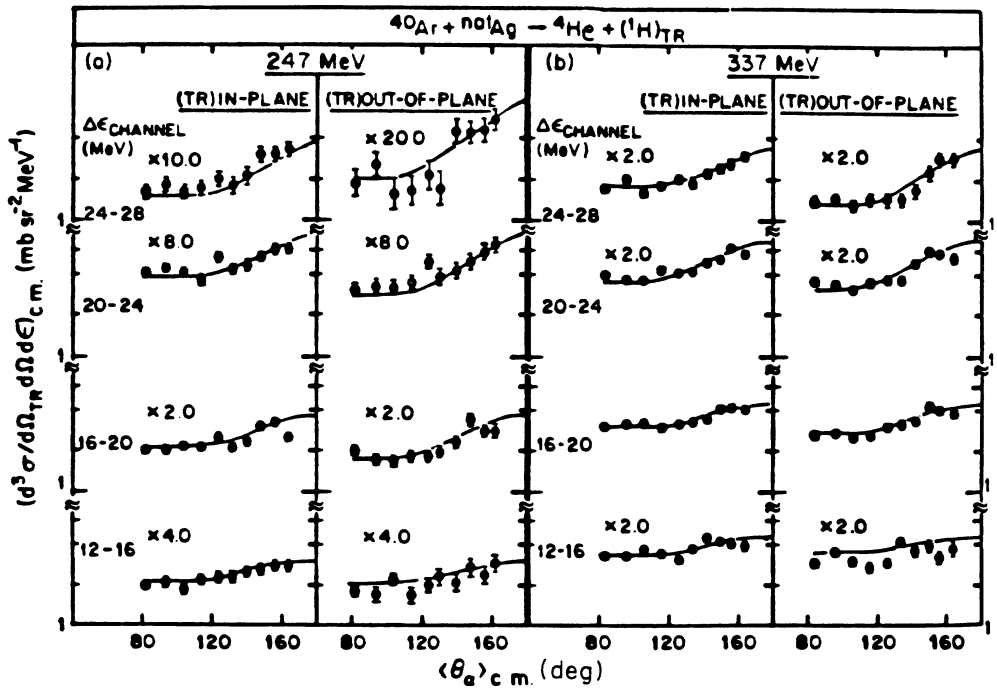

FIG. 8. Measured ^{4}He-^{1}H correlation distributions (in the c.m.) as a function of the energy bin ΔE_α. Solid curves were calculated as described in Fig. 2(b), i.e., $0 < J < l_{ER}$ and $\langle E^* \rangle = \frac{2}{3} E_{CN}$.

Fig. 5 and discussed below. The relevant parameters which characterize these fits are summarized in Table VII. The detailed fits shown in Figs. 7 and 8, indicate that the "basic" evaporation model is very successful in describing the angular distributions provided one assigns an effective emission barrier of 13.2 MeV for ^{4}He (see Table VII).

B. Relation to energy spectra

The energy distributions for the light charged particles present a more interesting challenge as shown in Figs. 9 and 10. The smooth curves in these figures represent reaction simulations for a spherical emitter with spin zones $0-l_{ER}$ for ^{1,2,3}H-^{4}He and $35-l_{ER}$ for ^{4}He-^{4}He. To fit the high-energy slopes, a mean fractional excitation energy loss of $\frac{1}{3}$ (e.g., to neutron emission) was used in all cases. Of greater significance, however, are the effective emission barriers that were used. These were taken from the empirical systematics for fusion between ^{1}H or ^{4}He and cold target nuclei.[19] These fusion barriers (16.0 MeV for ^{4}He and 8.6 MeV for ^{1}H, ^{2}H, and ^{3}H) clearly overesti-

TABLE VII. Derived statistical properties of the ER composite-nucleus emitters. (A spherical nucleus was assumed for the evaluation of these properties.)

	337 (MeV)	247 (MeV)
$J^{\alpha\alpha}_{\rm rms}(\hbar)$[a]	51	47
$J^{p\alpha}_{\rm rms}(\hbar)$[a]	45	41
$\beta_2^{\alpha\alpha}(\alpha)$[b]	1.73	1.99
$\beta_2^{p\alpha}$(p)	0.35	0.40
$\beta_2^{p\alpha}(\alpha)$	1.55	1.72
$B^{\alpha\alpha}(\alpha)$(MeV)[c]	13.2	13.2
$B^{\alpha\alpha}_{fus}(\alpha)$(MeV)[de]	15.85	16.10
$B^{p\alpha}$(p)(MeV)[f]	6.0	6.0
$B^{p\alpha}_{fus}$(p)(MeV)[dg]	8.49	8.64
⟨FEL⟩[h]	0.33	0.33
τ^{ER}(MeV)[i]	2.55	1.90

[a]Root mean square spin of the emitter. For p-α correlations, calculations were performed with the spin zones (for ER's) indicated in Fig. 2; for α-α correlations, spin zones of $35-70\hbar$ ($29-67\hbar$) were employed in the calculations for 337(247) MeV ^{40}Ar.

[b]$\beta_2=(\hbar^2J^2/2\tau\mathcal{J})[\mu R^2/(\mathcal{J}+\mu R^2)]$.

[c]Effective evaporation barrier for ^{4}He (from fits to the data): α-α or p-α correlations.

[d]Empirical fusion barriers [Ref. 19]. The separate values indicated for 337 and 247 MeV arise from thermal expansion of the nucleus (Ref. 24).

[e]Barriers for ^{4}He: α-α or p-α correlations. Barriers for α-α correlations differ from those for p-α by $\approx$0.10 MeV.

[f]Effective evaporation barrier for ^{1}H (from fits to the data): p-α correlations.

[g]Barrier for ^{1}H: p-α correlations.

[h]Fractional excitation energy lost (FEL) to particle emission prior to the emission of ^{1}H or ^{4}He.

[i]Mean temperature of the daughter nucleus. These values also reflect the selected ⟨FEL⟩ values above.

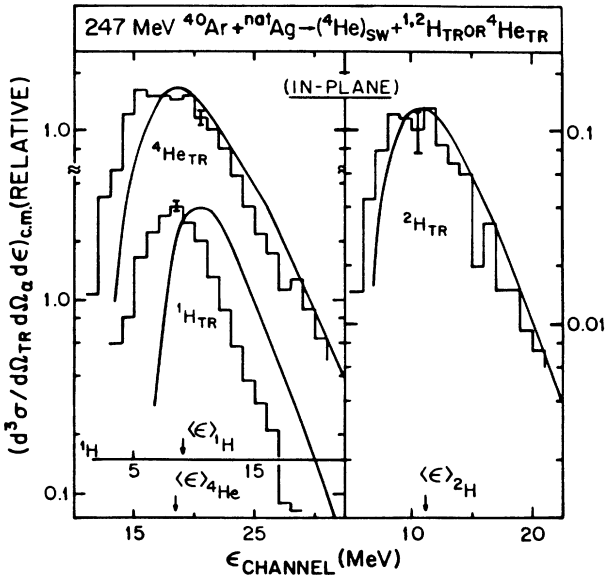

FIG. 9. Channel energy spectra for ^{1,2,3}H and ^{4}He production at $\langle\theta_{c.m.}\rangle=90°$ in coincidence with ^{4}He in either wedge 1 or 2 (247 MeV ^{40}Ar beam). Solid curves are simulations of evaporation from a spherical emitter with $\frac{2}{3}$ of its initial excitation energy, and a spin zone of $0<J<70\hbar$. Barriers for ^{1}H and ^{4}He were taken from Ref. 19, and those for ^{2}H and ^{3}H were set equal to that for ^{1}H. Average observed energies are indicated by arrows.

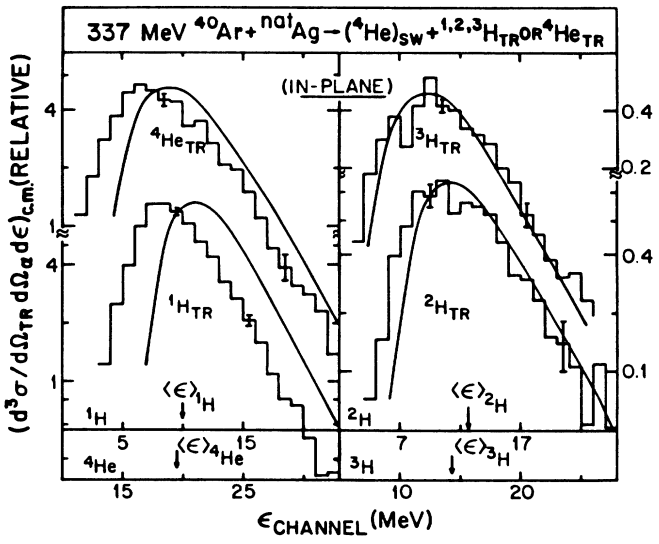

FIG. 10. Channel energy spectra for ^{1,2,3}H and ^{4}He production at $\langle\theta_{c.m.}\rangle=90°$ in coincidence with ^{4}He in either wedge 1 or 2 (337 MeV ^{40}Ar beam). Solid curves are simulations of evaporation from a spherical emitter with $\frac{2}{3}$ of its initial excitation energy, and a spin zone of $0<J<70\hbar$. Barriers for ^{1}H and ^{4}He were taken from Ref. 19, and those for ^{2}H and ^{3}H were set equal to that for ^{1}H. Average observed energies are indicated by arrows.

mate the effective evaporation barriers as illustrated in Figs. 9 and 10. The very good fits shown in Fig. 5 employed mean ^{4}He barriers of 13.2 MeV. For the protons a mean barrier of 6.0 MeV was required. Such deviations from the fusion barriers have been commonly attributed to deformation of the emitters.[5,15,19–22]

In analogy to the analysis carried out for the fragment-particle correlations,[7] a series of calculations was performed to explore the possible role of deformation in accounting for these rather low evaporation barriers. The code GANES was used to explore this possibility as described below.

C. Calculations for deformed emitters

The Monte Carlo method employed in the correlation calculations is described in.[8,9,5] Nonetheless, it is useful to reexamine some of the earlier results for particle evaporation from a deformed nucleus. The results for the evaporation of a single alpha particle are particularly illustrative. Figure 11 shows calculated mean c.m. energies and anisotropies versus emitter shape for two simple geometries (a) ideal coincidence (the emitter spin is fixed along the y axis) and (b) ideal singles (the emitter spin uniformly distributed at all azimuthal angles perpendicular to the beam or z axis). Note that the mean energies in Fig. 11(a) for 90° are identical to those in Fig. 11(b) at 0°. These two situations select only those particles emitted perpendicular to the emitter spin. The mean energies (and emission probabilities) for 90° in Fig. 11(b) (ideal singles) lie between those for 90° and 0° in ideal coincidence. This is a natural consequence of the averaging over the spin orientations. This averaging results in smaller energy changes with angle and smaller anisotropies for the singles calculation.

The geometrical constraints for particle-particle coincidences lie somewhere between those for ideal coincidence and ideal singles. If the trigger applies a very strong alignment constraint then the calculated results will be very close to those for ideal coincidences. If the trigger applies a very weak alignment constraint, then the calculated results will be very close to those for ideal singles. For intermediate trigger situations the calculated results will lie between those for ideal singles and ideal coincidences. The proton triggers provide a rather weak alignment constraint while the alpha triggers provide a much stronger constraint.

The role of emitter shape can also be examined from Fig. 11. It is evident that shape changes do not affect the anisotropies very strongly for this reaction. As discussed in Ref. 9, the role of the deformation on barrier reduction is essentially offset by a reduction in the centrifugal or spinoff effect due to the increasing moment of inertia. By contrast the mean emission energies do exhibit a shape dependence that must be explored with care.

In Fig. 12 a series of calculated quantities (open sym-

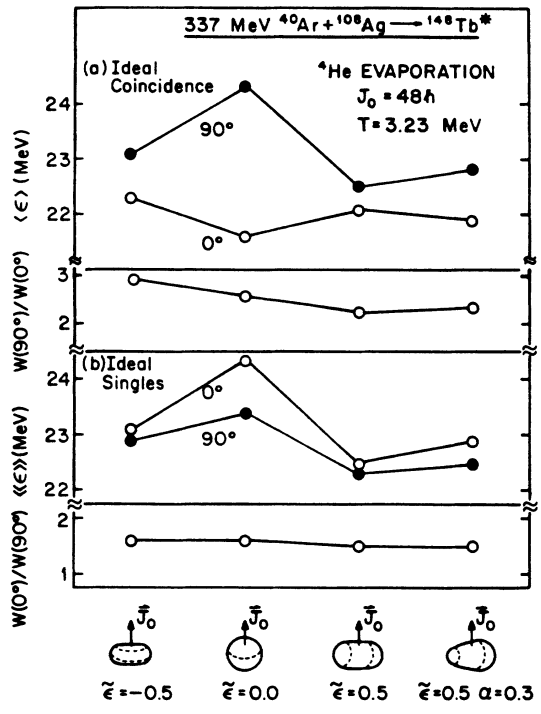

FIG. 11. Shape dependence of various average quantities for the reaction 337 MeV ^{40}Ar+^{108}Ag→^{148}Tb*(τ=3.2 MeV, J_0=49ħ. (a) Ideal coincidence experiment. (b) Ideal singles experiments (after Ref. 9).

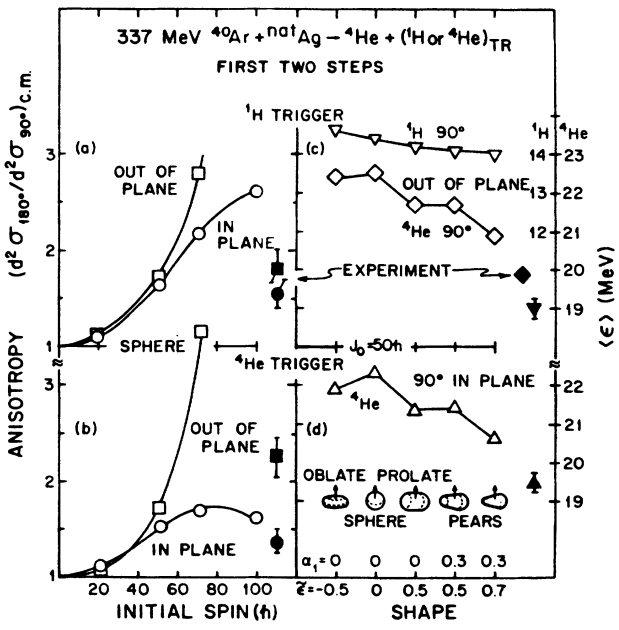

FIG. 12. Calculated anisotropies [(a) and (b)] vs spin for a spherical emitter with ^{1}H or ^{4}He trigger particles. Calculated average channel energies ⟨ϵ⟩ [(c) and (d)] vs shape (parameters $\tilde{\epsilon}$ and α_1) for an initial spin of 50ħ. The Cassini parameter $\tilde{\epsilon}$ is related to the axis ratio while the dipolar asymmetries (into pear shapes) are given by α_1 (as discussed in Ref. 23). Experimental values are given as solid points to be compared to the corresponding open symbols. Calculations are for a trigger detector at 90° c.m., in-plane.

bols) are compared to analogous observed quantities (solid symbols) obtained with particle-particle coincidence constraints (^{1}H-^{4}He or ^{4}He-^{4}He). The calculations were made for the idealized c.m. geometry of Fig. 1(b), which is very similar (but not identical) to that of the experiment [Fig. 1(a)]. The correlation anisotropies [Figs. 12(a) and (b)] represent the ratios $(d^2\sigma_{(180°)}/d^2\sigma_{(90°)_{c.m.}}$ for ^{4}He particles as triggered in-plane or out-of-plane by ^{1}H [Fig. 12(a)] or by a second ^{4}He [Fig. 12(b)]. The observed anisotropies are taken from Fig. 2. For the proton trigger [Fig. 12(a)], the data are consistent with the calculation for a root-mean-square spin of $\approx 50\hbar$. For the ^{4}He trigger [Fig. 12(b)], the average of the in-plane and out-of-plane anisotropies is also consistent with $\approx 50\hbar$, but the observed ratio is not consistent with the calculations. By decreasing the mean excitation energy and raising the spin (both increase the anisotropy), one can account for these anisotropies as shown by the smooth curves in Figs. 2(a) and (b). The consideration of deformed shapes does not impose any significant alterations to this pattern. Thus one can conclude that these particles are evaporated from composite nuclei that lead to ER's with spins up to $\approx 70\hbar$.

The comparison of calculated mean energies to those observed is shown in Figs. 12(c) and (d). Here the emitter shape *is* important to the calculated energies for ^{4}He. Spherical emitters give mean energies ≈ 22 MeV for the alphas. Strongly deformed emitters give ≈ 21 MeV compared to ≈ 20 MeV observed—a significant but not a very big difference. For protons, however, the calculated mean energies are all ≈ 14 MeV compared to ≈ 10 MeV observed. These are the same discrepancies illustrated in Figs. 9 and 10 as "spherical shifts." The conclusion from these results is that emitter deformations are probably not the only cause of the low observed particle energies. For protons no deformation seems strong enough; for alphas the extent of the deformation required seems to be unimaginable for an emitter that does not subsequently undergo fission. In short, one must search elsewhere for an explanation.

The above results cannot be reconciled to evaporation calculations (from GANES or any other code) without some basic changes in the philosophy of the model. Static deformations are not sufficient. Hence, the challenge is to explain these low barriers or, in other words, the shifts in the energy spectra as indicated in Figs. 9 and 10. The basic idea for a possible explanation of these findings is presented in the next few paragraphs.

The suggestion is that the reaction dynamics are not adequately treated. Recall that statistical evaporation models[12] have traditionally assumed that all dynamical information is contained in the transmission coefficients (i.e., cross sections for the inverse reactions). If the emitter nucleus has a density profile that differs from cold nuclei in fusion reactions, this difference must be addressed. Indeed the small swelling expected for a hot equilibrated Fermi gas *has* been included in the barriers that were used for the calculated spectra.[8,9,24]

Clearly, an additional physical ingredient is needed in the model; the following plausible scenario suggests a possibility for this missing ingredient. At the time of impact, the orbits of many nucleons in both projectile and target must be tremendously disturbed. Many particles must be scattered into transitory orbits of very high excitation from which extensive rearrangements must occur in the drive toward complete equilibrium. Extensive energy mixing can be achieved in relatively few collisions, and thus thermalization can be expected to be rapidly achieved.[25] However, the density distribution of this composite nuclear system might have a transient stratosphere of "high altitude orbits" that will relax quite rapidly into the density profile of a normal Fermi gas with the shape of a rotating liquid drop at equilibrium. The disparities shown in Figs. 9 and 10 could be rationalized if evaporationlike emission takes place while this diffuse nuclear stratosphere is relaxing. If so, the basic driving and restraining forces for particle and cluster emission can still be the number of available channels and the Coulomb barrier. However, two new dynamical features are needed to model such quasievaporative emission: (a) the probability for cluster formation and (b) reduction of the barriers from those characteristic of fusion to those appropriate to the orbits of the excited particles.

The very low proton energies in Figs. 9 and 10 suggest that many protons are emitted from the far extremities of the transitory density distribution (≈ 8.6 to 6.0 MeV barrier reduction or ≈ 1.5 fm beyond the normal fusion barrier). By contrast, the more normal deuteron and triton energies suggest that their preformation probability may demand a higher density region than those of the protons, i.e., characterized by orbits of much smaller radial extent. The rather low alpha particle energies (16.0–13.2 MeV barrier reduction) suggest emission from orbits of rather high altitude but much less than those for protons. The strong binding energy of ^{4}He may well give a great preference to its preformation compared to that for ^{3}H and ^{2}H. In summary, these observations suggest a new sort of nuclear surface excitation and relaxation that has not previously come under detailed scrutiny.

VI. SUMMARY

In this paper many results have been presented, for particle-particle correlations between ^{1,2,3}H or ^{4}He and ^{4}He. The major findings can be briefly summarized as follows: (1) Charged particle chains of two or three protons and/or two or three alpha particles are often produced in reactions that lead to ER's. (2) The coincidence cross sections as well as the angular distributions for ^{4}He are consistent with the notion that the multiplicity increases with spin for ^{4}He but decreases with spin for the protons. (3) The angular correlations of both ^{1}H and ^{4}He are very well described by a standard semiclassical evaporation model. (4) The energy distributions can also be very well described if one employs effective emission barriers strongly reduced from those for fusion of cold nuclei. These reductions are 16.0–13.2 MeV for ^{4}He, 8.5–6.0 for ^{1}H, 8.5–7.7 for ^{2}H and essentially no reduction for ^{3}H. (5) Massive deformation of the emitters could conceivably account for the ^{4}He spectra but not for the ^{1}H spectra or the trend from ^{1}H to ^{2}H to ^{3}H. (6) A new form of excitation and evaporationlike decay is proposed. A hot, very diffuse nuclear surface is formed that

promotes evaporative decay prior to its relaxation. The low barriers reflect the radial extent of this transitory, diffuse surface. Preformation probabilities limit ^{2}H And ^{3}H to regions of higher nuclear density and smaller radial extent.

ACKNOWLEDGMENTS

The staff of the Lawrence Berkeley Laboratory SuperHilac is gratefully acknowledged. For helpful discussions we thank R. McGrath, M. Prakash, J. Boger, A. Narayanan, and A. Elmaani. This work was supported by the Division of Nuclear Physics, Office of High Energy and Nuclear Physics, U.S. Department of Energy.

APPENDIX

In Sec. IV, an analysis was made based on the singles cross sections [σ_S^p(ER) and σ_S^α(ER)] and double coincidence cross sections [$\sigma_{DC}^{\alpha\alpha}$(ER), σ_{DC}^{pp}(ER), and $\sigma_{DC}^{p\alpha}$(ER)] that are associated with the ER's. These ER cross sections were obtained by correcting analogous *observed* cross sections (σ_S^p, σ_S^α, $\sigma_{DC}^{\alpha\alpha}$, σ_{DC}^{pp} $\sigma_{DC}^{p\alpha}$) for contributions from reactions involving FF and QF fragments. The corrections for the singles cross sections have been discussed in the text. Consequently, the major concern here is with the double coincidence corrections. We show here the analysis for 337 MeV ^{40}Ar; a similar treatment was made for 247 MeV ^{40}Ar.

For the double coincidences there are two independent methods for these corrections. Most simply, one can subtract the measured triple coincidence cross sections $\sigma_{TC}^{f\alpha\alpha}$, σ_{TC}^{fpp}, and $\sigma_{TC}^{fp\alpha}$ (Tables I and II) from the measured values for particle-particle double coincidences. Alternatively, these contributions can be estimated from the fragment-particle coincidence multiplicities given in Tables I and II. Assuming independent emission probabilities for FE and CE emission, the cross section for producing a chain of two α particles in FF or QF reactions can be expressed as follows:

$$\sigma_{DC}^{\alpha\alpha}(FF)=\sigma_{FF}M_{CE}^{\alpha}M_{FE}^{\alpha}$$
$$=(520\text{ mb})(0.30)(0.28)=43\text{ mb}\ , \quad \text{(A1)}$$

and

$$\sigma_{DC}^{\alpha\alpha}(QF)=\sigma_{QF}M_{CE}^{\alpha}M_{FE}^{\alpha}$$
$$=(700\text{ mb})(0.14)(0.27)=26\text{ mb}\ , \quad \text{(A2)}$$

where σ_{FF} and σ_{QF} are the cross sections for producing FF and QF products respectively; M_{CE}^{α} and M_{FE}^{α} are the respective multiplicities (average) for composite emission and fragment emission. Similarly for chains of two protons

$$\sigma_{DC}^{pp}(FF)=\sigma_{FF}M_{CE}^{p}M_{FE}^{p}$$
$$=(520\text{ mb})(0.25)(0.64)=85\text{ mb}\ , \quad \text{(A3)}$$

and

$$\sigma_{DC}^{pp}(QF)=\sigma_{QF}M_{CE}^{p}M_{FE}^{p}$$
$$=(700\text{ mb})(0.18)(0.45)=58\text{ mb}\ . \quad \text{(A4)}$$

In the same spirit, it is also reasonable to assume memory loss for charged particle emission from fragments 1 and 2 after scission. This assumption leads to the relationship

$$\sigma_{DC}^{\alpha\alpha}(FF)=\sigma_{FF}\left[\frac{M_{FE}^{\alpha}}{2}\right]^2=520(\tfrac{0.28}{2})^2=10\text{ mb}\ . \quad \text{(A5)}$$

For the protons

$$\sigma_{DC}^{pp}(FF)=520(\tfrac{0.64}{2})^2=54\text{ mb}\ . \quad \text{(A6)}$$

In order to determine σ(ER), the FF and QF contributions must be subtracted from the overall particle-particle double-coincidence cross sections

$$\sigma_{DC}(ER)=\sigma_{DC}-\sigma_{DC}(FF)-\sigma_{DC}(QF)\ . \quad \text{(A7)}$$

Hence, for the alpha particles

$$\sigma_{DC}^{\alpha\alpha}(ER)=1142-2(43+26+10)=984\text{ mb}\ , \quad \text{(A8)}$$

and for the protons

$$\sigma_{DC}^{pp}(ER)=2115-2(85+58+54)=1271\text{ mb}\ . \quad \text{(A9)}$$

The factor of 2 in the above equations [Eqs. (A7) and (A8)] is derived from particle indistinguishability and the neglect of alpha or proton chains ≥ 3 for FF or QF reactions. This neglect seems justified by the relatively small average multiplicities for FF and QF (see Table I). For this same reason, it seems justified to neglect the two particle chains from either CE or FE that are associated with either FF or QF. The very good agreement between the measured and estimated triple coincidence cross sections in Table III also serves as a good test of the assumptions described above.

Another important double coincidence measurement is that for protons with α's (i.e., $\sigma_{DC}^{p\alpha}$). The measured value for all reactions is $\sigma_{DC}^{p\alpha}=1474$ mb. This value must also be corrected for the contributions from FF and QF reactions. The contribution from one CE and one FE particle is as follows:

$$\sigma_{DC}^{p\alpha}(FF)=\sigma_{FF}(M_{CE}^{\alpha}M_{FE}^{p}+M_{CE}^{p}M_{FE}^{\alpha})$$
$$=520\text{ mb}[(0.30)(0.64)+(0.28)(0.25)]$$
$$=137\text{ mb}\ , \quad \text{(A10)}$$

and

$$\sigma_{DC}^{p\alpha}(QF)=\sigma_{QF}(M_{CE}^{\alpha}M_{FE}^{p}+M_{CE}^{p}M_{FE}^{\alpha})$$
$$=700\text{ mb}[(0.14)(0.45)+(0.27)(0.18)]$$
$$=79\text{ mb}\ . \quad \text{(A11)}$$

One might also wish to consider ^{4}He emission to be independent of ^{1}H emission in CE and/or FE emission. For this assumption one obtains

$$\sigma'^{p\alpha}_{DC}(FF)=\sigma_{FF}(M^{\alpha}_{CE}M^{p}_{CE}+M^{\alpha}_{FE}M^{p}_{FE})$$
$$=520\text{ mb}[(0.30)(0.25)+(0.14)(0.32)]$$
$$=62\text{ mb}, \quad \text{(A12)}$$

$$\sigma'^{p\alpha}_{DC}(QF)=\sigma_{QF}(M^{\alpha}_{CE}M^{p}_{FE}+M^{\alpha}_{FE}M^{p}_{FE})$$
$$=700\text{ mb}[(0.14)(0.18)+(0.27)(0.45)]$$
$$=104\text{ mb}. \quad \text{(A13)}$$

Now the value of $\sigma^{p\alpha}_{DC}$ can be obtained for the set of ER reactions

$$\sigma^{p\alpha}_{DC}(ER)=\sigma^{p\alpha}_{DC}-\sigma^{p\alpha}_{DC}(FF)$$
$$-\sigma'^{p\alpha}_{DC}(FF)-\sigma^{p\alpha}_{DC}(QF)-\sigma'^{p\alpha}_{DC}(QF)$$
$$=1474-137-62-79-104=1092\text{ mb}. \quad \text{(A14)}$$

Again, one can verify these estimates by comparing the measured triple coincidnece cross section of $\sigma^{fp\alpha}_{TC}=295$ mb ($\pm 30\%$) to the estimated value of 382 mb. (The other estimated cross sections are listed along with the measured ones in Table III).

---

*Permanent address: Bhabha Atomic Research Centre, Nuclear Physics Division Trombay 400085, Bombay, India.
†Permanent address: Department of Chemistry, Middle East Technical University, Ankara, Turkey.
‡Permanent address: Istituto di Fisica Sperimentale, Mostra d'Oltremare, Napoli 80125, Italy.
§Permanent address: Data Systems Division, International Business Machines, Kingston, NY 12401.
**Permanent address: Department of Physics, Hope College, Holland, MI 49423.

[1]H. C. Britt, B. H. Erkkila, R. H. Stokes, H. H. Gutbrod, F. Plasil, R. L. Ferguson, and M. Blann, Phys. Rev. C **13**, 1483 (1976).
[2]Z. Majka, D. G. Sarantites, L. G. Sobotka, K. Honkanen, E. L. Dines, L. A. Adler, L. Ze, M. L. Halbert, J. R. Beene, D. C. Hensley, R. P. Schmitt, and G. Nebbia, Phys. Rev. Lett. **58**, 322 (1987).
[3]Z. Majka, M. E. Brandan, D. Fabris, K. Hagel, A. Menchaca-Rocha, J. B. Natowitz, G. Nebbia, G. Prete, B. Sterling, and G. Viesti, Phys. Rev. C **35**, 2125 (1987).
[4]T. Kuang-Hsi, T. Dossing, C. Gaarde, and J. S. Larsen, Nucl. Phys. **A316**, 189 (1979).
[5]R. Lacey, N. N. Ajitanand, J. M. Alexander, D. M. de Castro Rizzo, G. F. Peaslee, L. C. Vaz, G. La Rana, M. Kaplan, D. J. Moses, W. Parker, D. Logan, and P. DeYoung, J. Phys. (Paris) Colloq. **C-4**, 289 (1986).
[6]R. Lacey, N. N. Ajitanand, J. M. Alexander, D. M. de Castro Rizzo, P. DeYoung, M. Kaplan, L. Kowalski, G. La Rana, D. Logan, D. J. Moses, W. E. Parker, G. E. Peaslee, and L. C. Vaz, Phys. Lett. **B191**, 253 (1987).
[7]R. Lacey, N. N. Ajitanand, J. M. Alexander, D. M. de Castro Rizzo, G. F. Peaslee, L. C. Vaz, M. Kaplan, M. Kildir, G. LaRana, D. J. Moses, W. E. Parker, D. Logan, M. S. Zisman, P. DeYoung, and L. Kowalski, Phys. Rev. C **37**, 2539 (1988).
[8]N. N. Ajitanand, R. Lacey, G. F. Peaslee, E. Duek, and J. M. Alexander, Nucl. Instrum. Methods **A243**, 111 (1986).
[9]N. N. Ajitanand, G. La Rana, R. Lacey, D. J. Moses, L. C. Vaz, G. F. Peaslee, D. M. deCastro Rizzo, M. Kaplan, and J. M. Alexander, Phys. Rev. C **34**, 877 (1986).
[10]T. Ericson and V. Strutinski, Nucl. Phys. **8**, 284 (1958); T. Ericson and V. Strutinski, *ibid.* **9**, 689 (1959).
[11]A. C. Douglas and N. MacDonald, Nucl. Phys. **13**, 382 (1959).
[12]T. Ericson, Adv. Phys. **9**, 423 (1960).
[13]T. Dossing, Licentiat thesis and unpublished notes, University of Copenhagen, 1977.
[14]L. C. Vaz, J. M. Alexander, and N. Carjan, Z. Phys. **A324**, 331 (1986).
[15]D. J. Moses, M. Kaplan, M. Kildir, D. R. G. Logan, G. La Rana, W. E. Parker, R. Lacey, G. F. Peaslee, J. M. Alexander, N. N. Ajitanand, L. C. Vaz, and M. S. Zisman, Nucl. Phys. **A465**, 339 (1987), D. J. Moses, *et al.*, Phys. Rev. C **36**, 422 (1987).
[16]M. M. Fowler and R. C. Jared, Nucl. Instrum. Methods **124**, 341 (1975).
[17]W. Hauser and H. Feshbach, Phys. Rev. **87**, 336 (1952).
[18]G. F. Peaslee, Ph.D. thesis, State University of New York at Stony Brook, 1988.
[19]L. C. Vaz and J. M. Alexander, Z. Phys. **A318**, 231 (1984).
[20]L. Schad, H. Ho, G. Y. Fan, B. Lindl, A. Pfoh, R. Wolski, and J. P. Wurm, Z. Phys. **A318**, 179 (1984).
[21]E. Holub, D. Hilscher, G. Ingold, U. Jahnke, H. Orf, H. Rossner, W. P. Zank, W. U. Schroder, H. Gekmmeke, K. Keller, L. Lassen, and W. Lucking, Phys. Rev. C **33**, 143 (1986).
[22]G. La Rana, D. J. Moses, W. E. Parker, M. Kaplan, D. Logan, R. Lacey, John M. Alexander, and R. J. Welberry, Phys. Rev. C **35**, 373 (1987).
[23]V. V. Pashkevich, Nucl. Phys. **A169**, 275 (1971).
[24]X. S. Chen, C. Ngô, and E. Thomasi, M. Barranco, X. Vinas, and H. Ngô, Nucl. Phys. **A401**, 143 (1983).
[25]G. D. Harp, J. M. Miller, and B. J. Berne, Phys. Rev. **165**, 1166 (1968).